CMS Physics Analysis Summary

Contact: cms-pag-conveners-susy@cern.ch 2012/11/17

Scalar Top Quark Search with Jets and Missing Transverse Momentum in pp Collisions at $\sqrt{s} = 7\,\text{TeV}$

The CMS Collaboration

Abstract

A search for scalar top quarks is presented in final states with jets and missing transverse momentum. The data sample of proton–proton collisions used corresponds to an integrated luminosity of 4.98 fb^{-1} collected at $\sqrt{s} = 7$ TeV with the CMS detector at the LHC. The data is found to be in agreement with the predicted backgrounds. Exclusion limits are set in simplified models with the top squark decaying to an undetected particle and jets, either through an on-shell top quark, or through a chargino. For a massless undetected particle, we respectively exclude at 95 percent C.L. top squark masses between 295 and 375 GeV and between 280 and 375 GeV, the latter for a chargino at 75 percent of the top squark mass.

1 Introduction

The standard model is the most successfully tested description of nature to date – yet it is known to be incomplete. It offers no explanation for the observed dark-matter content of the universe [1]. In addition, if the boson recently observed at the LHC [2, 3] is found to be at the origin of electroweak symmetry breaking, then the so-called hierarchy problem arises, requiring fine-tuning of the quantum effects which drive the Higgs scalar's mass to the Planck scale. Requiring the standard model not to exhibit such unnatural fine-tuning therefore implies the need for a mechanism to stabilize the mass of the Higgs boson. Supersymmetric theories with conservation of so-called R-parity offer a possible explanation for these basic questions [4]. The lightest supersymmetric particle (LSP) in such a theory would be stable, can be neutral, and therefore is a good dark-matter candidate. Furthermore, the supersymmetric partner particles cancel the divergence of large radiative corrections to the Higgs boson mass, allowing it to remain naturally light near the electroweak scale.

To date, no supersymmetric particles have been experimentally observed. Current limits from the LHC [5, 6] place gluino masses above $\sim$ 1.1 TeV for some decay topologies in the decoupled squark limit, and first and second generation squark masses above $\sim$ 800 GeV in the decoupled gluino limit. Supersymmetry must therefore be a broken symmetry, and the cancellation of the radiative corrections to the Higgs-boson mass cannot be exact. Due to the large standard model Yukawa coupling of the top quark, supersymmetric scalar partners to the right- and left-handed top quarks ($\tilde{t}_R$, $\tilde{t}_L$) play the dominant role in naturalizing quantum effects to the Higgs boson mass. Hence, supersymmetry as a solution to the hierarchy problem theoretically motivates the top squark, to be of a similar mass scale as the top quark [7, 8]. Existing limits on the production of light scalar top quark pairs from the Tevatron [9–12] and the LHC [13–17] only probe a small portion of the possible phase space, with the range $m(\tilde{t}) \sim 225$ to 500 GeV excluded for low LSP masses and a few specific decay topologies.

Motivated by the large branching fraction to quarks, and the lack of intrinsic missing transverse momentum ($\not\!\!E_{\mathrm{T}}$) in the fully-hadronic top-pair background, this search concentrates on hadronic top-squark-decay final states with jets, b-quark jets, and $\not\!\!E_{\mathrm{T}}$. Two possible top squark decay channels are considered within the context of simplified models [18–20]: $\tilde{t} \to t\tilde{\chi}^0 \to bW^+\tilde{\chi}^0$, through an on-shell top decay, and $\tilde{t} \to b\tilde{\chi}^+ \to bW^+\tilde{\chi}^0$, through an intermediate chargino, both leading to a $b\bar{b}qqqq+\not\!\!E_{\mathrm{T}}$ final state. In this analysis, no assumption is made about the presence of on-shell top quarks in the top squark decays, thereby retaining sensitivity for both decay modes. In order of decreasing importance, the relevant standard model backgrounds to this search are: $t\bar{t}$ production with a $W^{\pm} \to \ell^{\pm}\nu$ decay, invisible $Z \to \nu\nu$ decays accompanied by jets, and multijet production from QCD. All other SM production processes can be considered to be part of one of these background categories. In this analysis each of these three background components is predicted using data control samples.

This article is organised as follows. In Section 2, the detector is described, along with the physics object reconstruction and event samples used. The event selection for the considered search regions is detailed in Section 3. In Section 4, the prediction of the background is discussed. Results are compared to data in Section 5 and interpreted for the considered new-physics models.

2 Detector, objects and datasets

The central feature of the CMS apparatus is a superconducting solenoid 13 m in length and 6 m in diameter, which provides an axial magnetic field of 3.8 T. The bore of the solenoid is instru-

mented with various particle detection systems. Charged particle trajectories are measured by the silicon pixel and strip tracker, covering $0 < \phi < 2\pi$ in azimuth and $|\eta| < 2.5$, where the pseudorapidity η is defined as $\eta = -\ln[\tan(\theta/2)]$, with θ being the polar angle of the particle's momentum with respect to the counterclockwise beam direction. A lead-tungstate crystal electromagnetic calorimeter (ECAL) and a brass/scintillator hadronic calorimeter (HCAL) surround the tracking volume and cover the region $|\eta| < 3$. Quartz/steel forward hadron calorimeters extend the coverage to $|\eta| \leq 5$. The steel return yoke outside the solenoid is instrumented with gas-ionisation detectors which are used to identify muons. The detector is nearly hermetic, allowing for momentum balance measurements in the plane transverse to the beam directions. A detailed description of the CMS detector can be found elsewhere [21].

All physics objects are reconstructed in a global event description, using a particle-flow technique [22]. This algorithm identifies and reconstructs individually the particles produced in the collision, namely charged and neutral hadrons, photons, muons, and electrons, by combining the information from the tracking system, the calorimeters, and the muon system. The missing transverse momentum vector $\vec{\not{E}}_{\mathrm{T}}$ is computed as the negative vector sum of all reconstructed particles, without further corrections. All these particles are further clustered into jets using the anti-k_T algorithm with a distance parameter of 0.5 [23] from FASTJET [24]. Subtraction of energy deposits from simultaneous pileup collisions is performed using vertex compatibility of reconstructed charged hadrons, and in a second step by means of in situ estimation of the pileup energy density in the event. As over-subtraction may induce spurious mis-balancing of momentum sums, pileup correction is performed only for jet momenta as used for kinematic cuts and counting jet multiplicities. Jet energies are corrected for the non-linear calorimeter response using calibration factors derived from simulation. For jets in data, an additional residual energy correction derived from data is applied [25]. Jets are identified to originate from b-quarks using an algorithm that combines the information on track impact parameters and identified secondary vertices within jets, even when full vertex information is not available [26]. The b-tagging efficiencies in simulation are corrected to match data measurements [27].

This analysis is performed using a data sample with an integrated luminosity of $4.98\,\mathrm{fb}^{-1}$ of pp collisions at 7 TeV, collected in 2011 by the CMS detector at the LHC at CERN. Events are only considered if they pass online selections requiring the presence of two jets, and large missing transverse momentum calculated from all calorimeter deposits. These trigger requirements are found to select on average 95% of events with $\not{E}_{\mathrm{T}} = 175\,\mathrm{GeV}$, reaching quickly 100% at higher values of $\not{E}_{\mathrm{T}}$.

Several effects related to e.g. electronics noise, beam backgrounds, etc., are known to potentially lead to an apparent but unphysical large value of $\not{E}_{\mathrm{T}}$. The events used in this analysis have been pruned of such mis-reconstruction effects, while ensuring that the inefficiency so induced on the selection of processes with genuine $\not{E}_{\mathrm{T}}$ stays below 1%. Additionally, a requirement is imposed to reject events where a large amount of energy is deposited in badly functioning ECAL crystals ($\sim$1% of the total).

Several Monte-Carlo (MC) simulated event samples are used throughout the analysis. The MADGRAPH [28] generator was used for the $\mathrm{t\bar{t}}$, W+jets, Z+jets and γ+jets processes, while single-top production was generated using POWHEG [29], and both PYTHIA [30] and MADGRAPH was used to generate multijet QCD events. Other processes, like $\mathrm{t\bar{t}Z}$, were found to be very small. On all events, PYTHIA was subsequently used to perform parton showering, while where relevant tau leptons were decayed using TAUOLA [31]. The detector interaction and response for all background samples were simulated in detail using GEANT [32]. The top squark signal samples were generated using PYTHIA, with normalization to the next-to-leading order

plus next-to-leading-logarithm cross section [33–37]. In this case a parametrized simulation of the detector response is used. For these signal simulations the top squark mass is varied up to 700 GeV and the LSP mass from 0 GeV up to the kinematical limit for the considered top squark decays.

3 Event selection

The main signal targeted by this analysis is supersymmetric top squark pair production, with each top squark either decaying through an on-shell top quark or via a chargino. In Figure 1, the signal production diagrams corresponding to the considered simplified models are shown. The subset of events leading to a fully-hadronic final state are in either case characterized by the presence of six jets in the final state, two of which originate from b quarks, accompanied by missing transverse momentum from the LSPs.

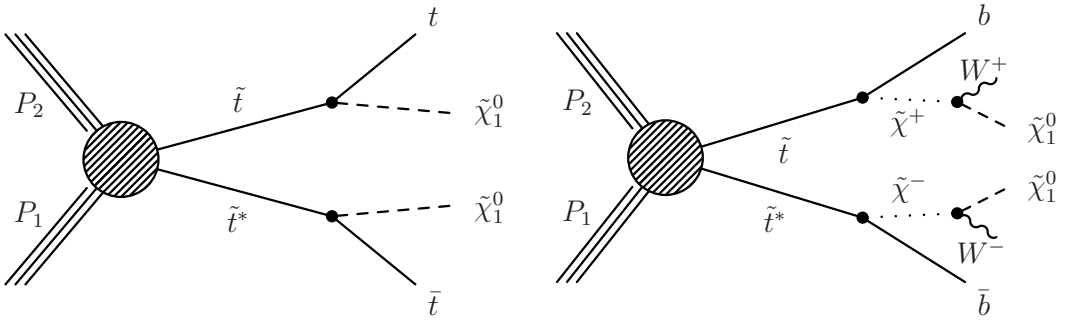

Figure 1: Diagrams representing the simplified models of direct top squark pair production considered, either with a decay to an on-shell top quark (left), or via a chargino (right).

We define a high statistics sample, referred to as the baseline selection, from which dedicated search regions are developed. This sample consists of events with at least five jets with $p_{\mathrm{T}} \geq 30\,\mathrm{GeV}$ and $|\eta| \leq 2.4$, of which at least one should be identified as a b jet. The leading three jets should in addition have $p_{\mathrm{T}} \geq 50\,\mathrm{GeV}$. The requirement on the missing transverse momentum value is $\not{E}_{\mathrm{T}} > 175\,\mathrm{GeV}$, to be in the asymptotically efficient region with respect to the online event selection requirement. To suppress events with strong mismeasurement of a single high-p_{T} jet, $\vec{\not{E}}_{\mathrm{T}}$ should be separated in ϕ from the first, second, and third highest-p_{T} jets within $|\eta| \leq 4.7$, by $\Delta\phi(\vec{\not{E}}_{\mathrm{T}}, \mathrm{jet}) > 0.5$, 0.5, and 0.3 respectively. Finally, events containing muon, electron, or tau leptons are vetoed with dedicated selections, hence suppressing backgrounds with real $\not{E}_{\mathrm{T}}$ arising from a leptonic W-boson decay.

The identification criteria for the electron and muon veto were designed to be as loose as possible, aiming for maximal rejection of prompt lepton backgrounds, while maintaining a $< 10\%$ loss of the fully-hadronic top squark signal. With two b-quarks per signal event, electrons and muons from B-meson decays are the dominant cause for signal events to be vetoed. The main variables found to discriminate between leptons from prompt or B decay sources are the transverse and longitudinal impact parameters of the lepton track relative to the interaction vertex, and the isolation of the lepton from the rest of the activity in the event. In this analysis, a novel definition of isolation sum has been developed that uses information about the spatial distribution of energy deposits around the lepton of interest. This so-called "directional isolation" calculates the sum of particle transverse momenta in a cone around the lepton by weighting their momenta with the square of the angle in the $\eta - \phi$ plane between each particle and the p_{T}-weighted centroid of all particles contributing to the isolation. The weighting enhances the

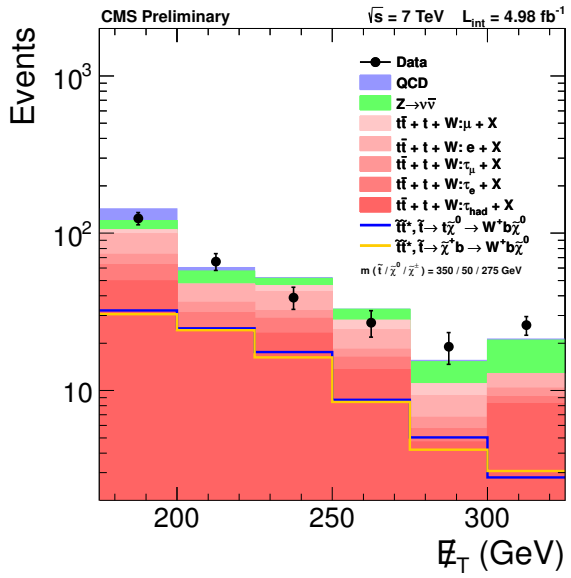

Figure 2: $\not\!\!E_T$ distribution for events passing the baseline selection. Data yields are compared to the background predictions discussed throughout this note. Two signal models are shown overlaid on the background.

magnitude of the isolation sum for leptons inside the core of jets, as arise from B-meson decays, as opposed to prompt leptons that randomly overlap with—but are mostly still just outside—of the jet cones. The muon and electron selection criteria optimized using these isolation and vertex compatibility requirements were found to provide 40% additional rejection of the leptonic top and W backgrounds (including $\tau \to e$ or μ) on top of what is achieved with more conventional e and μ vetoes.

In order to suppress backgrounds with hadronic tau leptons from W decay, a veto is placed on events with a τ-like jet. Such jets are identified to have $p_T > 15\,\text{GeV}$ and $|\eta| < 2.4$, to fail the b-jet identification criteria, to have few charged particles in a small cone around the jet direction, and to have a small jet broadness. In addition, these jets should be compatible with coming from a W decay, by giving rise to a transverse mass formed by the jet and $\not\!\!E_T$ below 90 GeV. After baseline selection, this tau-lepton veto rejects 50% of the semileptonic $t\bar{t}$ events with a hadronically-decaying tau lepton, while retaining 80% of the top squark signal with a top squark mass of 400 GeV.

Backgrounds and signal yields according to MC simulated samples, as well as yields in data collected by the search trigger, are summarized in Table 1 for various stages of the event selection. The $\not\!\!E_T$ distribution after the baseline selection is shown in Figure 2. The dominant background arises from semileptonically decaying $t\bar{t}$, W+jets and single top production, where the lepton either is out of kinematic acceptance, isn't reconstructed, or otherwise doesn't satisfy the veto's criteria for isolation and/or identification. The second largest background is Z boson production where the boson decays invisibly, generating thus a high $\not\!\!E_T$ more or less equal to the boson p_T. A third background component consists of multijet events, from QCD production but also hadronically decaying $t\bar{t}$. The $\not\!\!E_T$ in such events arises from rare severe jet mismeasurements surviving the $\Delta\phi(\not\!\!E_T, \text{jet})$ cuts.

Jet counting and $\not\!\!E_T$ are two of the most discriminating variables utilized in this search. Depending on the top squark and LSP masses, sometimes either the higher $\not\!\!E_T$ or jet multiplicity provides better signal-versus-background separation. Therefore this analysis is optimised ver-

Table 1: Number of expected simulated and observed data events for an integrated luminosity of 4.98 fb^{-1}.

	Baseline	Loose	Medium	Tight
$\mathrm{t\bar{t}}_{\mathrm{lepton+jets}}(\tau_\mathrm{h})$	128.1	40.0	24.4	18.4
$\mathrm{t\bar{t}}_{\mathrm{lepton+jets}}(\mu+\tau_\mu)$	24.0 + 21.5	6.9 + 6.6	4.0 + 3.0	3.0 + 2.8
$\mathrm{t\bar{t}}_{\mathrm{lepton+jets}}(\mathrm{e}+\tau_\mathrm{e})$	37.5 + 27.4	11.3 + 8.3	6.9 + 5.0	5.0 + 3.4
$\mathrm{W}(\tau_\mathrm{h})$	8.8	1.9	0.9	0.7
$\mathrm{W}(\mu+\tau_\mu)$	1.8 + 1.2	0.6 + 0.9	0.3 + 0.6	0.2 + 0.2
$\mathrm{W}(\mathrm{e}+\tau_\mathrm{e})$	3.0 + 0.5	1.6 + 0.2	1.0 + 0.2	0.5 + 0.0
Single top	15.3	3.9	2.0	1.8
$\mathrm{t\bar{t}}_{\mathrm{di-lepton}}(\tau_\mathrm{h},\tau_\mathrm{h}/\ell)$, $\ell=\mathrm{e},\mu,\tau_\mathrm{e},\tau_\mu$	10.5	3.0	1.7	1.3
$\mathrm{t\bar{t}}_{\mathrm{di-lepton}}(\ell,\ell)$, $\ell=\mathrm{e},\mu,\tau_\mathrm{e},\tau_\mu$	2.1	0.6	0.3	0.3
Total missing lepton	281.7	85.8	50.3	37.6
$\mathrm{Z}(\nu\nu)$	25.7	15.3	8.5	3.3
QCD multijets	27.7	4.1	2.2	0.3
$\mathrm{t\bar{t}}_{\mathrm{all-hadronic}}$	2.3	1.0	0.8	0.8
MC total	337.4	106.2	61.8	42.0
$\tilde{\mathrm{t}}\bar{\tilde{\mathrm{t}}}^*$, $\tilde{\mathrm{t}}\to\mathrm{t}\tilde{\chi}^0\to\mathrm{bW}^+\tilde{\chi}^0$ all	110.7	57.3	40.4	32.5
$\tilde{\mathrm{t}}\bar{\tilde{\mathrm{t}}}^*$, $\tilde{\mathrm{t}}\to\mathrm{t}\tilde{\chi}^0\to\mathrm{bW}^+\tilde{\chi}^0$ all-hadronic $m_{\tilde{\mathrm{t}}/\tilde{\chi}^0}=350/50\,\mathrm{GeV}$	95.6	48.9	35.1	29.2
$\tilde{\mathrm{t}}\bar{\tilde{\mathrm{t}}}^*$, $\tilde{\mathrm{t}}\to\mathrm{b}\tilde{\chi}^+\to\mathrm{bW}^+\tilde{\chi}^0$ all	102.9	45.0	31.2	24.2
$\tilde{\mathrm{t}}\bar{\tilde{\mathrm{t}}}^*$, $\tilde{\mathrm{t}}\to\mathrm{b}\tilde{\chi}^+\to\mathrm{bW}^+\tilde{\chi}^0$ all-hadronic $m_{\tilde{\mathrm{t}}/\tilde{\chi}^+/\tilde{\chi}^0}=350/275/50\,\mathrm{GeV}$	91.1	40.4	28.4	22.4
Data	301	123	80	49

sus so-called staircase cuts, where events are selected passing either of a set of cuts on $\not\!\!E_\mathrm{T}$ and jet multiplicity. An additional requirement considered in the search optimisation is the minimal angle between b-tagged jets and the $\not\!\!E_\mathrm{T}$, $\min|\Delta\phi(\vec{\not\!\!E}_\mathrm{T},\vec{p}_{\mathrm{T},b})|$, which is enhanced at small values for $\mathrm{t\bar{t}}$ background events, while showing little correlation for signal.

The optimisation maximizes sensitivity to a given signal, taking into account systematic uncertainties on both signal and background. Because of the relatively low signal-over-background ratio, the systematic uncertainties on the background play a crucial role in the optimisation. In the derivation of the above search regions, projected uncertainties for the $\mathrm{t\bar{t}}$ background have been used. After optimisation, three search regions were identified, each utilizing some combination of cuts in the above-mentioned variables. These regions are named "loose", "medium" and "tight", with each tighter region a subset of the looser ones.

Loose: $\min|\Delta\phi(\vec{\not\!\!E}_\mathrm{T},\vec{p}_{\mathrm{T},b})|\geq 1.0$ and $(\not\!\!E_\mathrm{T}\geq 175\wedge n_j\geq 7)\vee(\not\!\!E_\mathrm{T}\geq 200\wedge n_j\geq 5)$

Medium: $\min|\Delta\phi(\vec{\not\!\!E}_\mathrm{T},\vec{p}_{\mathrm{T},b})|\geq 1.0$ and $(\not\!\!E_\mathrm{T}\geq 175\wedge n_j\geq 7)\vee(\not\!\!E_\mathrm{T}\geq 200\wedge n_j\geq 6)\vee(\not\!\!E_\mathrm{T}\geq 250\wedge n_j\geq 5)$

Tight: $\min|\Delta\phi(\vec{\not\!\!E}_\mathrm{T},\vec{p}_{\mathrm{T},b})|\geq 1.0$ and $(\not\!\!E_\mathrm{T}\geq 175\wedge n_j\geq 7)\vee(\not\!\!E_\mathrm{T}\geq 200\wedge n_j\geq 6)$

4 Background determination

4.1 Tau and lost leptons from W bosons and top quarks

The background arising from processes like $\mathrm{t\bar{t}}$ and W+jets is dominated by events in which one W boson decays to an electron, muon, or tau lepton, and where the lepton goes out of kinematic acceptance, is not reconstructed, or passes the corresponding veto. This background is predicted from data using a muon+jets control sample orthogonal to the signal sample. A translation is made from this sample to the signal regions by means of a technique of embedded simulated leptons. The event sample thus obtained describes the full kinematics of the background.

The muon+jets control sample is selected by requiring exactly one muon using the directional isolation and with tight vertex compatibility requirements. Other selections are done such that all events that can pass $\not{E}_\mathrm{T}$ and jet requirements after embedding the simulated lepton are present in the control sample. The main source of background to the control sample arises from events with the selected muon coming from $\mathrm{W} \to \tau\nu_\tau \to \mu\nu_\mu\nu_\tau$ decay. To account for this background, the control sample is corrected as a function of the muon p_T with a factor obtained from the ratio of $W \to \tau_\mu\nu_\tau$ to $\mathrm{W} \to \mu\nu$ in simulated $\mathrm{t\bar{t}}$ muon+jets events. The contamination of the control sample by QCD multijet events was evaluated to be very small. Other backgrounds are subtracted using simulation.

To use this control sample as a representation of the true $\mathrm{W} \to \ell\nu$ ($\ell = \mathrm{e}, \mu, \tau$) production within kinematical acceptance, corrections need to be applied for the inefficiency of the muon reconstruction and of the control sample identification and isolation requirements. The former is a very small effect and it is taken from simulation, while the latter is estimated in the data using Z tag-and-probe efficiency measurements parametrized as a function of the muon p_T, and the angular distance from the muon to the nearest jet.

The procedure of embedding consists of taking out the muon from the event, simulating at the event's vertex a lepton with same momentum as the original muon's, and merging all the reconstructed particles from that simulated lepton back into the original data event. To avoid bias from embedding a lepton in the direction of an already isolated muon, the lepton is simulated using the original muon's momentum, but with the azimuthal angle ϕ mirrored around the azimuthal direction of the W boson, taken as the vector sum of the muon and the $\not{E}_\mathrm{T}$ momenta. This flips both the $\not{E}_\mathrm{T}$ and muon p_T around the W axis in the transverse plane, thus preserving the W p_T, and ensuring a proper description of the jet-environment around the lepton. For the tau-lepton embedding, the simulation with the `PYTHIA` generator [30] was interfaced with the `Tauola` library [31] to ensure an accurate description of the tau decays, including the polarization in W decays. Here, the same control-sample event is being reused multiple times to sufficiently sample the tau-decay phase space. After embedding, objects like jets and $\not{E}_\mathrm{T}$ are rebuilt and all search cuts, including the lepton vetoes, are then directly applied to evaluate the expected background.

This embedding procedure makes it possible to mimic the data environment of the background in terms of jets, pileup, etc, and is observed to predict well the MC expectation when applying it to simulation. Deviations from the MC truth observed when executing the method on simulated events are corrected for and propagated as a closure uncertainty to the result. The prediction using this method in data, to obtain the backgrounds like $\mathrm{t\bar{t}}$, containing a $\mathrm{W} \to \ell\nu$ decay, is shown in Table 2 for all search regions, along with all considered uncertainties.

Apart from the level of closure assessed with simulation as a function of number of jets and $\not{E}_\mathrm{T}$, additional corrections are taken into account, with corresponding uncertainties, when applying

Table 2: Total prediction for the lost e, μ and τ backgrounds, along with all considered uncertainties.

Event selection	Baseline	Loose	Medium	Tight
Prediction	$235.4 \pm 13.9\ ^{+39.5}_{-29.5}$	$62.2 \pm 6.6\ ^{+10.7}_{-8.1}$	$39.5 \pm 5.3\ ^{+7.5}_{-6.1}$	$27.9 \pm 4.2\ ^{+5.8}_{-4.9}$
Statistical uncertainty	$\pm$ 5.9 %	$\pm$ 10.7 %	$\pm$ 13.4 %	$\pm$ 14.9 %
Closure uncertainty	$\pm$ 6.9 %	$\pm$ 7.7 %	$\pm$ 10.2 %	$\pm$ 12.0 %
Electron η correction uncertainty	$\pm$ 3.0 %	$\pm$ 3.3 %	$\pm$ 5.8 %	$\pm$ 7.9 %
Lepton efficiency uncertainty	$\pm$ 1.0 %	$\pm$ 1.0 %	$\pm$ 1.0 %	$\pm$ 1.0 %
τ_μ subtraction uncertainty	$^{+15\%}_{-10\%}$	$^{+15\%}_{-10\%}$	$^{+15\%}_{-10\%}$	$^{+15\%}_{-10\%}$

the method on data. The number of events with prompt leptons outside the considered p_T and η acceptance is predicted using an estimate of the out-to-in fraction in simulation. The effect on the electron and muon veto requirements of embedding simulation in data is evaluated by comparing efficiency measurements in $Z \to \ell\ell$ data events and in the same data events where a simulated $Z \to \ell\ell$ decay with same Z momentum is embedded. For the electron reconstruction, which is sensitive to the jet environment, a similarly obtained correction needs to be applied to translate from the efficiency in an empty simulated event to the efficiency in a signal-like data environment. A lepton efficiency uncertainty is associated to cover related systematic effects. An observed non-closure in the prediction of the lost electron η distribution is corrected through reweighting, and the full correction is taken as uncertainty. Finally, for the subtraction of the τ_μ component of the control sample, an uncertainty is assessed to cover remaining kinematic differences between the muons from prompt or τ decay.

4.2 Invisible decays of Z bosons

The established method [38] for the prediction of the background from Z bosons decaying into neutrinos, using a phenomenological translation of photon+jets events to events with a Z boson, suffers from the absence of a solid theoretical model for high jet multiplicity and heavy flavour in the final state. Instead, we use a $Z \to \mu\mu$ control sample opportunely rescaled by the differences between the target and the control sample in acceptance and Z branching ratio. To overcome the statistical penalty, no b-tag is required in the control sample. Rather, a translation is applied to the event fraction which has at least one b-tagged jet, using a correction factor derived from a photon+jets control sample, which allows to estimate this fraction at a higher jet multiplicity.

The dimuon control sample is selected from events collected with single-muon triggers, and by asking for exactly two muons with tight isolation and identification requirements to have an invariant mass between 60 and 120 GeV. The background, mostly from $t\bar{t}$, is extracted and then subtracted, by fitting the dimuon invariant mass in an extended mass window. The photon sample is composed of events passing single-photon triggers, which are fully efficient in our phase space of interest. Photons are selected with criteria which yield a very pure sample, with photon isolation sums corrected for deposits from pileup collisions. In order to mimic the jet and $\not{E}_T$ characteristics in $Z \to \nu\bar{\nu}$ events, the muons and photon in these samples are not accounted for when calculating the $\not{E}_T$ and the number of jets.

A key ingredient for the prediction is the fraction χ_b of events which contain at least one b-tagged jet. This quantity is measured as a function of the number of jets n_{jets} in events from the $Z(\to \mu\mu)$+jets and γ+jets control samples, for events with boson $p_T > 175$ GeV. To overcome the low statistics at high jet multiplicity, $\chi_b(n_{jets})$ is determined in the γ+jets control sample.

Although the γ and Z sample may have a different absolute scale of the b-quark content, e.g. due to the relative couplings of the bosons with the b quarks, the trend as a function of jet multiplicity is expected to be the same. Indeed, at high jet multiplicity gluon radiation and subsequent splitting in $b\bar{b}$ pairs becomes the dominant b-jet production mode for both processes. Therefore, the photon sample is used to measure χ_b, after which it is normalised to the $Z \to \mu\mu$ sample using as reference the number of events with three and four jets. The overall uncertainty assigned to the normalisation is coming from the statistics of the sample and has been evaluated to be of 14%.

Furthermore, χ_b is observed to be linearly dependent on the number of jets, in both the data and simulation samples for both γ and Z. This linear dependence is also confirmed at lower boson p_T threshold. To improve the precision on the knowledge of the fraction of the events with a b-tagged jet, the $\chi_b(n_{jets})$ distribution is fitted with a linear function, which is then used for extrapolation into the high n_{jets} search regions. The systematic uncertainty on the fit choice is folded in as a χ_b shape uncertainty.

The described method cannot predict the full physics of $Z \to \nu\bar{\nu}$ events, since the presence of a b-tagged jet is predicted only on average. Hence, any kinematic requirement on b jets needs to be evaluated on average and applied as a correction factor to the final prediction of the background. The efficiency of the $\Delta\phi(b, \not{E}_T)$ selection cut in this analysis is extracted from simulation for each of the search regions, after validation at low jet multiplicity and low Z transverse momentum using the muon sample, and in a region at high jet multiplicity for high boson p_T using the photon sample. The values used for this correction, along with the corresponding systematic uncertainty are reported in Tab. 4.

In Table 3 the predictions of the $Z \to \nu\bar{\nu}$ background for the baseline and the three search regions are reported. The systematic uncertainties for each region are displayed in the same table, covering the already mentioned

Table 3: Summary of the prediction of the $Z(\nu\nu)$+jets background in all search regions. Yields from simulation are normalised to leading-order cross section.

	Baseline	Loose	Medium	Tight
MC expectation	26 ± 2	15 ± 2	8.5 ± 1.4	3.3 ± 0.9
MC prediction	28 ± 3	16 ± 2	9.9 ± 1.7	4.0 ± 1.1
Prediction from data	$47 \pm 8 \pm 9$	$27 \pm 6 \pm 5$	$18 \pm 5 \pm 4$	$12 \pm 5 \pm 3$

Table 4: Summary of the corrections and the corresponding systematic uncertainties on the $Z(\nu\nu)$+jets background prediction in all search regions.

	Baseline	Loose	Medium	Tight
Acceptance (X BR) correction	10.6 ± 7 %	10.2 ± 8 %	9.8 ± 9 %	10.7 ± 14 %
$\Delta\phi(B, \not{E}_T)$ efficiency correction	–	0.81 ± 0.02	0.79 ± 0.03	0.76 ± 0.05
χ_B shape (from MC)	5%	5%	7%	16%
χ_B normalisation	14%	14%	14%	14%
Binning of Data/MC efficiency scale factor	2%	2%	2%	2%
Background-subtraction factor (data only)	$0.85^{+0.06}_{-0.07}$	$0.87^{+0.06}_{-0.09}$	$0.90^{+0.06}_{-0.11}$	$0.87^{+0.08}_{-0.13}$

4.3 QCD multijets

The idea behind the QCD multijet prediction is to reweight Monte Carlo simulated multijet events, so that key distributions agree with observations in various data control regions. These

simulated events are then used to predict the QCD background by applying selection criteria in the usual manner. There are two general aspects that are brought into agreement: first the particle-level description of multijet production, and secondly the modelling of detector (mis-)measurement effects that cause these otherwise well-balanced events to enter the high-$\not\!\!E_{\mathrm{T}}$ search regions. The simulated sample is corrected by applying a series of event weights (scale factors) defined as the ratio of data over simulated yields in distributions of interest and in appropriate control regions. The sequence of corrections is as follows.

First, the true multijet production kinematics are reweighted to a low pile-up data sample collected with H_{T} triggers. In order to ensure a good description of all kinematic quantities that affect the probability of multijet events to enter the search region, a set of variables are examined that include event jet multiplicities, p_{T} and η spectra of various p_{T}-ranks of jets, angular correlations i.e. $\Delta\eta$ and $\Delta\phi$ between jets, as well as the vector sum momenta of soft jets. As these quantities are often highly correlated due to the underlying physics process, it is often necessary to parametrise yields simultaneously in a few variables. Scale factors as a function of particle-level ("true") versions of the variables are then solved for using an unfolding method based on Bayes' theorem [39], obtaining what the simulated yields should be in order to match data. These scale factors are applied as multiplicative corrections on the weights of the simulated events. The procedure is then iterated to fix a next set of variables, and is seen to converge in a stable manner to $\sim 10\%$ data-MC agreement in all reweighted distributions.

The sub-population of events with production of one or more b-quark jets is of special relevance to this analysis. It is furthermore important for jet resolution and b-tagging efficiency to distinguish between "mono-b" jets consisting of the fragmentation products of a single b quark, vs. "multi-b" jets which are comprised of two or more b quarks. The yield of data events with multi-b jets is obtained in a subset of the H_{T}-triggered sample with exactly one b-tagged jet, by fitting simulated templates to observed distributions for the b-tagged jet: its charged particle multiplicity, number of reconstructed secondary vertices, and number of tracks with displaced impact parameters. This gives a scale factor for multi-b jet yields as a function of the b-jet p_{T}, which is used to correct the simulated multi-b production cross-section. After this the true cross-section for production of events with one or two mono-b jets is unfolded from the data yield of events with one and two b-tagged jets. The simulated events are then reweighted to match this cross-section.

Second, to correct for discrepancies between jet resolutions in data versus simulation, a $\not\!\!E_{\mathrm{T}}$ trigger is used to collect a high $\not\!\!E_{\mathrm{T}}$, low $\Delta\phi(\not\!\!E_{\mathrm{T}}, \mathrm{jet})$ control region. Events in this data sample are predominantly from multijet production, and particularly favour having exactly one strongly mismeasured jet, i.e. the one nearest to $\vec{\not\!\!E}_{\mathrm{T}}$ in ϕ. The latter is referred to as the probe jet in such events. The recoil momentum, i.e. the vector sum momenta of all the other jets, is a good estimator of the true momentum of the probe jet as the sum momenta of jets in multijet production events should cancel out in the absence of mismeasurements. As such the recoil response $p_{\mathrm{T,probe}}/p_{\mathrm{T,recoil}}$ is highly similar to the jet resolution $p_{\mathrm{T,probe}}/p_{\mathrm{T,true}}$, and is unfolded to obtain scale factors for the jet resolution in a similar way as for the other scale factors above. In order to account for jet and detector properties that induce a difference in resolution shapes, these scale factors are obtained in various bins of $p_{\mathrm{T,recoil}}$, and classifying jets by whether they are b-tagged or not, and if they are in regions of the ECAL with non-functional channels.

The "raw" predicted QCD background yield is obtained as the sum of weights of simulated events that pass various search region cutflows, where each event weight has been multiplied by the abovementioned scale factors. The final prediction in Table 5 is further multiplied by bias corrections described below. Systematic uncertainties for the QCD prediction are assessed

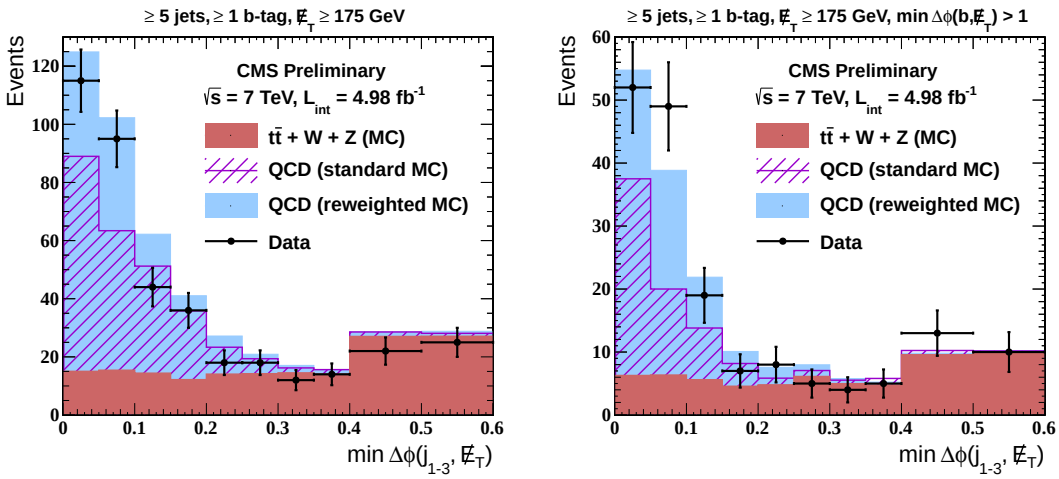

Figure 3: Distributions of minimum $\Delta\phi$ between the leading three jets and $\not\!\!E_{\mathrm{T}}$, for events with ≥ 5 jets, ≥ 1 b-tagged jet, $\not\!\!E_{\mathrm{T}} \geq 175\,\mathrm{GeV}$, and additionally a $\min|\Delta\phi(\vec{\not\!\!E}_{\mathrm{T}}, \vec{p}_{\mathrm{T},b})| \geq 1$ requirement for the figure on the right. The out-of-the-box simulation versus the reweighted QCD prediction is compared to the data yield in these plots. All QCD distributions are shown stacked on top of the non-QCD contribution.

by examining its agreement with data yields in QCD-enhanced control regions with events passing a $\not\!\!E_{\mathrm{T}}$ trigger. The closure level is defined as the ratio of the predicted over observed QCD yields, after subtracting from the latter the top, Z, and W-boson contributions as expected from simulation. In the ≥ 5 jets, $\min|\Delta\phi(\not\!\!E_{\mathrm{T}}, \text{jet 1-3})| < 0.15$, and ≥ 1 b-tag region, the closure level is within $\pm 20\%$ of unity as a function of $\not\!\!E_{\mathrm{T}}$, indicating soundness of the jet resolution correction procedure. After a $\min|\Delta\phi(\vec{\not\!\!E}_{\mathrm{T}}, \vec{p}_{\mathrm{T},b})| \geq 1.0$ selection, some tension away from unity has been observed for progressively higher jet multiplicities. However, for the most relevant regions the agreement is comparable to the statistical uncertainty of the data—see Figure 3. The overall closure level in the $\not\!\!E_{\mathrm{T}}$ and jet multiplicity regions required by the search are measured to be in the range of 0.9 to 1.4 (statistically compatible with unity) in the bulk of the search regions, and 2.2 ± 0.8 in a tiny subset with ≥ 7 jets and $\min|\Delta\phi(\vec{\not\!\!E}_{\mathrm{T}}, \vec{p}_{\mathrm{T},b})| \geq 1.0$. The reciprocal of the closure levels are taken as multiplicative bias corrections for the various search regions, and the larger of the correction or its statistical uncertainty is propagated as a systematic uncertainty of the procedure. The total uncertainty is dominated by the statistics of the simulated QCD sample.

Table 5: Prediction for the QCD multijet background, along with the statistical and systematic uncertainties.

Event selection	Baseline	Loose	Medium	Tight
Raw prediction	30.2	5.0	4.2	4.6
Corrected prediction	25.9	5.6	6.2	5.9
Statistical uncertainty	± 88%	± 40%	± 61%	± 52%
Closure uncertainty	± 12%	± 22%	± 29%	± 30%

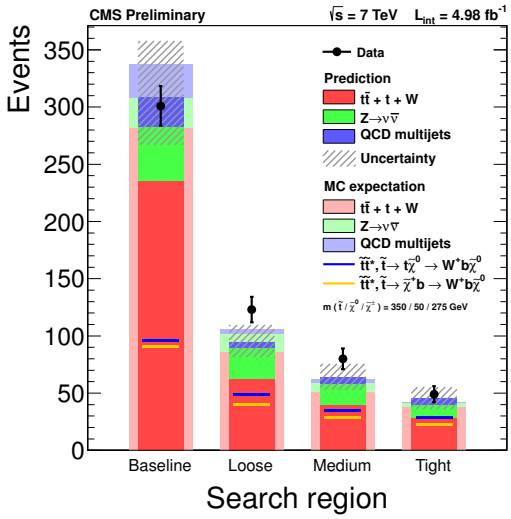

Figure 4: Number of events predicted, observed, and expected from simulation, for the various search regions, and split per background component. The hatched band represents the total uncertainty on the prediction. Two signal models are shown overlaid on the background.

5 Results and interpretation

In Table 6 all background predictions to the search are summarized, along with the expectations from Monte-Carlo simulation and the observations in data. In Figure 4 these results are summarized graphically.

Table 6: Number of predicted, expected from simulation, and observed events for the integrated luminosity of 4.98 fb^{-1}.

	Baseline	Loose	Medium	Tight
MC total	337.4	106.2	61.8	42.0
$\tilde{t}\bar{\tilde{t}}^*$, $\tilde{t} \to t\tilde{\chi}^0 \to bW^+\tilde{\chi}^0$ all-hadronic $m_{\tilde{t}/\tilde{\chi}^0} = 350/50$ GeV	95.6	48.9	35.1	29.2
$\tilde{t}\bar{\tilde{t}}^*$, $\tilde{t} \to b\tilde{\chi}^+ \to bW^+\tilde{\chi}^0$ all-hadronic $m_{\tilde{t}/\tilde{\chi}^\pm/\tilde{\chi}^0} = 350/275/50$ GeV	91.1	40.4	28.4	22.4
$t\bar{t}$, t and W+jets	$235.4 \pm 13.9\,^{+39.5}_{-29.5}$	$62.2 \pm 6.6\,^{+10.7}_{-8.1}$	$39.5 \pm 5.3\,^{+7.5}_{-6.1}$	$27.9 \pm 4.2\,^{+5.8}_{-4.9}$
$Z(\to \nu\nu)$+jets prediction	$47.3 \pm 8.4 \pm 8.5$	$26.9 \pm 5.5 \pm 5.4$	$18.2 \pm 4.8 \pm 3.6$	$11.5 \pm 4.7 \pm 3.4$
QCD multijets prediction	$25.9 \pm 22.7 \pm 3.0$	$5.6 \pm 2.2 \pm 1.3$	$6.2 \pm 3.8 \pm 1.8$	$5.9 \pm 3.1 \pm 1.8$
Total prediction	$308.6 \pm 27.9\,^{+40.6}_{-30.8}$	$94.7 \pm 8.9\,^{+12.1}_{-9.8}$	$63.9 \pm 8.1\,^{+8.5}_{-7.3}$	$45.3 \pm 7.0\,^{+7.0}_{-6.2}$
Data	301	123	80	49

The data is found to be in good agreement with the prediction. Therefore, the result of the search is interpreted as limits on new physics. Two simplified models of direct top squark pair production are considered, with the top squarks decaying to a final state of jets and LSPs, either through an on-shell top or via a chargino, as shown in Figure 1. All other particles are considered very heavy, effectively decoupled from the top squarks. As an input to the interpretation of the result in the considered simplified model, the systematic uncertainties on the signal efficiency are assessed. The uncertainty on the cross section is evaluated as a function of the top squark mass [40]. The luminosity uncertainty follows from the CMS 2011 luminosity meaurement [41]. The trigger uncertainty is conservatively taken to be 5% for selections with $\not\!\!E_T > 175$ GeV, and 1% elsewhere, where the trigger has reached full signal efficiency. The

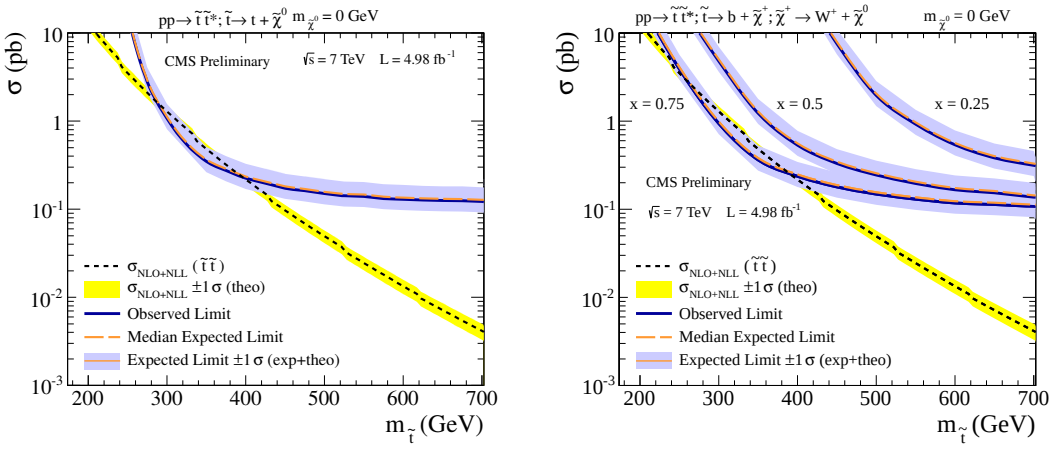

Figure 5: Expected and observed 95% CL upper limits (baseline selection) on the direct top-squark-pair production cross section, for the decay in $\tilde{t} \to t\tilde{\chi}^0$ (left) and $\tilde{t} \to b + \tilde{\chi}^+, \tilde{\chi}^+ \to W^+ + \tilde{\chi}^0$ (right), for $x = 0.25, 0.5, 0.75$, where $m_{\tilde{\chi}^\pm} = x \cdot m_{\tilde{t}} + (1 - x) \cdot m_{\tilde{\chi}^0}$.

uncertainty related to the removal or cleaning of anomalous $\not{E}_T$ events was determined to be within 2%. The combined lepton-veto uncertainty was estimated from data-MC comparisons to be 8%. Uncertainties from other sources are evaluated for each $(m_{\tilde{t}}, m_{\chi^0})$ point in the model's scan: jet energy scale (5-10%), jet energy resolution (1-5%), b-tag efficiency (1-4%) initial- and final-state radiation (5-20%), and effects due to parton distribution functions (<1%).

The expected and observed limits are calculated using both the frequentist CLs method, with a one-sided profile likelihood test statistic, and with the fast asymptotic CLs method. Statistical uncertainties are modelled as Poisson and systematic uncertainties as lognormal. The signal contamination of the background predictions is ∼100% of the leptonic signal yield, so the obtained results are equivalent to assuming only the presence of fully-hadronic signal and zero contamination on the predicted background yields. In Figure 5 the cross section upper limit for the baseline is shown overlaid on the top squark production cross section, as a function of the top squark mass, for $\tilde{\chi}^0 = 0$ GeV, for different decay-chain scenarios. Figure 6 displays the cross section upper limit in the $(m_{\tilde{t}}, m_{\tilde{\chi}^0})$ plane for the two top squark decay scenarios explored in this analysis.

6 Conclusion

A search for scalar top quarks was presented in final states with missing transverse momentum and a high jet multiplicity. Dedicated lepton vetoes were developed and applied, along with b-jet identification and kinematical constraints, to strongly suppress the backgrounds from $t\bar{t}$, W+jets, Z+jets and QCD multijet production. The remaining backgrounds are estimated as much as possible from the data. The observated data in the search regions is found to be in agreement with the predicted backgrounds. Exclusion limits are set in simplified models with either top squarks decaying to an undetected particle and an on-shell top quark, or top squarks decaying to ultimately the same final state, but through a chargino without an intermediate top. For a massless undetected particle and conservatively taking a $-1\,\sigma_{\text{theory}}$ lower bound on signal cross-sections, we respectively exclude at 95% CL top squark masses between 295 and 375 GeV and between 280 and 375 GeV, the latter for a chargino at 75% of the top squark mass.

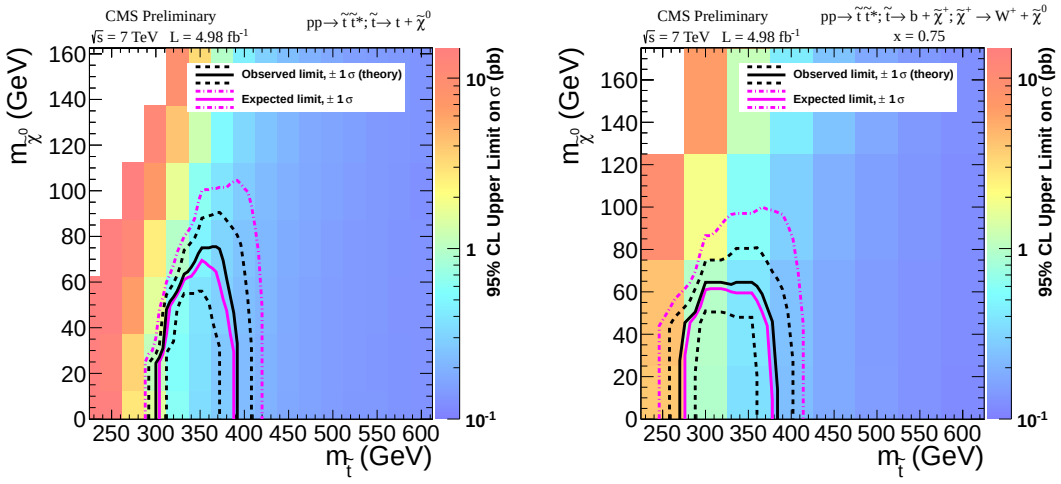

Figure 6: Expected and observed 95% CL upper limits (baseline selection) on the direct top-squark-pair production cross section, for the decay in $\tilde{t} \to t\tilde{\chi}^0$ (left) and $\tilde{t} \to b + \tilde{\chi^+}, \tilde{\chi^+} \to W^+ + \tilde{\chi}^0$, for $x = 0.75$ (right), where $m_{\tilde{\chi^\pm}} = x \cdot m_{\tilde{t}} + (1-x) \cdot m_{\tilde{\chi}^0}$.

References

[1] M. Drees and G. Gerbier, "Mini-Review of Dark Matter: 2012", arXiv:1204.2373.

[2] CMS Collaboration, "Observation of a new boson at a mass of 125 GeV with the CMS experiment at the LHC", *Phys.Lett.* **B716** (2012) 30–61, doi:10.1016/j.physletb.2012.08.021, arXiv:1207.7235.

[3] ATLAS Collaboration, "Observation of a new particle in the search for the Standard Model Higgs boson with the ATLAS detector at the LHC", *Phys.Lett.* **B716** (2012) 1–29, doi:10.1016/j.physletb.2012.08.020, arXiv:1207.7214.

[4] J. Wess and B. Zumino, "Supergauge Transformations in Four Dimensions", *Nucl. Phys. B* **70** (1974) 39, doi:{10.1016/0550-3213(74)90355-1}.

[5] CMS Collaboration, "Interpretation of Searches for Supersymmetry", *CMS-PAS-SUS-11-016* (2012).

[6] ATLAS Collaboration, "Search for squarks and gluinos with the ATLAS detector in final states with jets and missing transverse momentum using $4.7 fb^{-1}$ of sqrt(s) = 7 TeV proton-proton collision data", arXiv:1208.0949.

[7] R. Barbieri and D. Pappadopulo, "S-particles at their naturalness limits", *JHEP* **0910** (2009) 061, doi:10.1088/1126-6708/2009/10/061, arXiv:0906.4546.

[8] M. Papucci, J. T. Ruderman, and A. Weiler, "Natural SUSY Endures", *JHEP* **1209** (2012) 035, doi:10.1007/JHEP09(2012)035, arXiv:1110.6926.

[9] CDF Collaboration Collaboration, "Search for Scalar Top Quark Production in $p\bar{p}$ Collisions at $\sqrt{s} = 1.96$ TeV", arXiv:1203.4171.

[10] CDF Collaboration Collaboration, "Search for Pair Production of Supersymmetric Top Quarks in Dilepton Events from p anti-p Collisions at S**(1/2) = 1.96 TeV", *Phys.Rev.Lett.* **104** (2010) 251801, doi:10.1103/PhysRevLett.104.251801, arXiv:0912.1308.

[11] D0 Collaboration Collaboration, "Search for pair production of the scalar top quark in muon+tau final states", *Phys.Lett.* **B710** (2012) 578–586, doi:10.1016/j.physletb.2012.03.028, arXiv:1202.1978.

[12] D0 Collaboration Collaboration, "Search for pair production of the scalar top quark in the electron+muon final state", *Phys.Lett.* **B696** (2011) 321–327, doi:10.1016/j.physletb.2010.12.052, arXiv:1009.5950.

[13] ATLAS Collaboration, "Search for a supersymmetric partner to the top quark in final states with jets and missing transverse momentum at sqrt(s) = 7 TeV with the ATLAS detector", arXiv:1208.1447.

[14] ATLAS Collaboration, "Search for direct top squark pair production in final states with one isolated lepton, jets, and missing transverse momentum in sqrt(s) = 7 TeV pp collisions using 4.7 fb-1 of ATLAS data", arXiv:1208.2590.

[15] ATLAS Collaboration, "Search for a heavy top-quark partner in final states with two leptons with the ATLAS detector at the LHC", arXiv:1209.4186.

[16] CMS Collaboration, "Search for Supersymmetry with the Razor Variables at $\sqrt{s} = 7$ TeV", *CMS-PAS-SUS-11-016* (2012).

[17] CMS Collaboration, "Search for supersymmetery in final states with missing transverse energy and 0, 1, 2, or 3 b jets in 7 TeV pp collisions", *CMS-PAS-SUS-11-022* (2012).

[18] J. Alwall, P. Schuster, and N. Toro, "Simplified Models for a First Characterization of New Physics at the LHC", *Phys. Rev. D* **79** (2009) 075020, doi:10.1103/PhysRevD.79.075020, arXiv:0810.3921.

[19] J. Alwall, M.-P. Le, M. Lisanti et al., "Model-Independent Jets plus Missing Energy Searches", *Phys.Rev.* **D79** (2009) 015005, doi:10.1103/PhysRevD.79.015005, arXiv:0809.3264.

[20] LHC New Physics Working Group Collaboration, "Simplified Models for LHC New Physics Searches", *J.Phys.* **G39** (2012) 105005, doi:10.1088/0954-3899/39/10/105005, arXiv:1105.2838.

[21] CMS Collaboration, "The CMS Experiment at the CERN LHC", *JINST* **03** (2008) S08004, doi:10.1088/1748-0221/3/08/S08004.

[22] CMS Collaboration, "Particle–Flow Event Reconstruction in CMS and Performance for Jets, Taus, and $\not{E}_{\mathrm{T}}$", *CMS Physics Analysis Summary* **CMS-PAS-PFT-09-001** (2009).

[23] M. Cacciari, G. P. Salam, and G. Soyez, "The Anti-k_t Jet Clustering Algorithm", *JHEP* **04** (2008) 063, doi:10.1088/1126-6708/2008/04/063, arXiv:0802.1189.

[24] M. Cacciari, "FastJet: A Code for Fast k_t Clustering, and more", arXiv:hep-ph/0607071.

[25] CMS Collaboration, "Determination of Jet Energy Calibration and Transverse Momentum Resolution in CMS", *Submitted to JINST* (2011) arXiv:1107.4277.

[26] CMS Collaboration, "b-Jet Identification in the CMS Experiment", *CMS-PAS-BTV-11-004* (2012).

[27] CMS Collaboration, "Measurement of the b-tagging efficiency using $\mathrm{t\bar{t}}$ events", *CMS-PAS-BTV-11-003* (2012).

[28] J. Alwall et al., "MadGraph/MadEvent v4: The New Web Generation", *JHEP* **09** (2007) 028, doi:10.1088/1126-6708/2007/09/028, arXiv:0706.2334.

[29] S. Frixione, P. Nason, and C. Oleari, "Matching NLO QCD computations with Parton Shower simulations: the POWHEG method", *JHEP* **0711** (2007) 070, doi:10.1088/1126-6708/2007/11/070, arXiv:0709.2092.

[30] T. Sjöstrand, S. Mrenna, and P. Skands, "PYTHIA 6.4 Physics and Manual", *JHEP* **05** (2006) 026, doi:10.1088/1126-6708/2006/05/026, arXiv:hep-ph/0603175.

[31] N. Davidson, G. Nanava, T. Przedzinski et al., "Universal Interface of TAUOLA Technical and Physics Documentation", *Comput.Phys.Commun.* **183** (2012) 821–843, doi:10.1016/j.cpc.2011.12.009, arXiv:1002.0543.

[32] S. Agostinelli et al., "G4 – A Simulation Toolkit", *Nucl. Instrum. and Meth.* **506** (2003) 250, doi:10.1016/S0168-9002(03)01368-8.

[33] W. Beenakker, R. Hopker, M. Spira et al., "Squark and Gluino Production at Hadron Colliders", *Nucl. Phys.* **B492** (1997) 51, doi:10.1016/S0550-3213(97)00084-9, arXiv:hep-ph/9610490.

[34] A. Kulesza and L. Motyka, "Threshold resummation for squark-antisquark and gluino-pair production at the LHC", *Phys.Rev.Lett.* **102** (2009) 111802, doi:10.1103/PhysRevLett.102.111802, arXiv:0807.2405.

[35] A. Kulesza and L. Motyka, "Soft gluon resummation for the production of gluino-gluino and squark-antisquark pairs at the LHC", *Phys.Rev.* **D80** (2009) 095004, doi:10.1103/PhysRevD.80.095004, arXiv:0905.4749.

[36] W. Beenakker, S. Brensing, M. Kramer et al., "Soft-gluon resummation for squark and gluino hadroproduction", *JHEP* **0912** (2009) 041, doi:10.1088/1126-6708/2009/12/041, arXiv:0909.4418.

[37] W. Beenakker, S. Brensing, M. Kramer et al., "Squark and Gluino Hadroproduction", *Int.J.Mod.Phys.* **A26** (2011) 2637–2664, doi:10.1142/S0217751X11053560, arXiv:1105.1110.

[38] CMS Collaboration, "Search for New Physics with Jets and Missing Transverse Momentum in pp collisions at sqrt(s) = 7 TeV", *JHEP* **1108** (2011) 155, doi:10.1007/JHEP08(2011)155, arXiv:1106.4503.

[39] G. D'Agostini, "A Multidimensional unfolding method based on Bayes' theorem", *Nucl.Instrum.Meth.* **A362** (1995) 487–498, doi:10.1016/0168-9002(95)00274-X.

[40] M. Kramer, A. Kulesza, R. van der Leeuw et al., "Supersymmetry production cross sections in pp collisions at sqrts = 7 TeV", arXiv:1206.2892.

[41] CMS Collaboration, "Absolute Calibration of the Luminosity Measurement at CMS: Winter 2012 Update", *CMS-PAS-SMP-12-008* (2012).